Brazilian Journal
of Chemical
Engineering

ISSN 0104-6632
Printed in Brazil
www.abeq.org.br/bjche

Vol. 26, No. 01, pp. 63 - 74, January - March, 2009

STUDIES ON MIXED METAL OXIDES SOLID SOLUTIONS AS HETEROGENEOUS CATALYSTS

H. R. Arandiyan and M. Parvari*

Chemical Engineering Department, Iran University of Science and Technology,
Fax: + (98) (21) 7724-0495,Tehran, Iran.
E-mail: parvari@iust.ac.ir

(Submitted: May 5, 2008 ; Revised : June 21, 2008 ; Accepted : July 2, 2008)

Abstract - In this work, a series of perovskite-type mixed oxide $LaMo_xV_{1-x}O_{3+\delta}$ powder catalysts (x = 0, 0.1, 0.3, 0.5, 0.7, 0.9, and 1.0, with $0.5 < \delta < 1.5$), prepared by the sol–gel process and calcined at 750°C, provide an attractive and effective alternative means of synthesizing materials with better control of morphology. Structures of resins obtained during the gel formation process by FT-IR spectroscopy and XRD analysis showed that all the $LaMo_xV_{1-x}O_{3+\delta}$ samples are single phase perovskite-type solid solutions. The surface area (BET) between 2.5 - 5.0 m^2/g (x = 0.1 and 1.0 respectively) increases with increasing Mo ratio in the samples. They show high purity, good chemical homogeneity, and lower calcinations temperatures as compared with the solid-state chemistry route. SEM coupled to EDS and thermogravimetric analysis/differential thermal analyses (TGA/DTA) have been carried out in order to evaluate the homogeneity of the catalyst. Finally, the experimental studies show that the calcination temperature and Mo content exhibited a significant influence on catalytic activity. Among the $LaMo_xV_{1-x}O_{3+\delta}$ samples, $LaMo_{0.7}V_{0.3}O_{4.2}$ showed the best catalytic activity for the topic reaction and the best activity and stability for ethane reforming at 850°C under 8 bar.

Keywords: Mixed-oxide perovskite; Heterogeneous catalyst; La-Mo-V.

INTRODUCTION

The topic of this article is the study of perovskite systems and their application in catalysis. Many studies have been conducted with a view to rationalizing the design of perovskite catalysts, that is, to control the relationship between catalytic activity and chemical composition of crystalline ceramics known as perovskite-type mixed oxides. The archetypal perovskite is a mineral having the composition $CaTiO_3$. It was first described in the 1830s by the geologist Gustav Rose, who named it after the Russian mineralogist Count Lev Aleksevich von Perovski (Hazen, 1988). Although several different structures have been proposed for perovskites, an ideal perovskite-type oxide has a cubic ABO_3-type crystal structure in which divalent cations with a large ionic radius are coordinated by twelve oxygen atoms and occupy A-sites, and cations with a smaller tetravalent metal ionic radius are six-coordinated and occupy B-sites (Tanaka et al., 2001). One of the conditions for obtaining the perovskite structure is that electroneutrality must be maintained. The cation in the A-site might be mono-, di-, or trivalent, while that in the B-site might be tri-, tetra-, or pentavalent. The catalytic activity of such mixed-oxide perovskites can be greatly improved by partial substitution of the cations in the A- and/or B-sites. Moreover, the B-site cations may be partially reduced to form finely dispersed metallic species supported on the A-site cation oxide, which makes these materials ideal catalyst precursors for a range of reactions involving metals as active sites (Parvary et al., 2001; Goldwasser et al., 2005; Utaka et al., 2003; Goldwasser et al., 2003; Pietri et al., 2001). Cations A and B may be partially substituted by A' and B', respectively ($A_xA'_{1-x}B_yB'_{1-y}O_3$), and perovskites may have other stoichiometries or can be deficient in oxygen under well-defined conditions. Considering the need to preserve the structure and

*To whom correspondence should be addressed

maintain the contact between the A, B, and O ions, a tolerance factor (*t*) has been defined according to Equation (1), which is used to assess the stability of cubic structures (Goldschmidt et al., 1926).

$$t = \frac{r_A + r_O}{\sqrt{2}(r_B + r_O)} \quad (1)$$

where r_A, r_B, and r_O are the ionic radii. The cubic structure is only stable if the condition $0.8 \leq t \leq 1.0$ is met. The distance between the cations and oxygen depends only on the oxidation state of the cation and the nature of the occupied sites (octahedral or dodecahedral) (Parvary et al., 2001; Bernier, Mm. J. C., 1971). If the tolerance factor falls outside of this range, the cubic structure will be distorted and orthorhombic or rhombohedral structures will be obtained (Kattack et al., 1979).

A great many elements can form ideal or modified perovskites depending on the tolerance factor. This diversity within the perovskite family makes them of interest for practical applications as electronic materials, and hence a wealth of solid-state chemical information has been accumulated. Perovskites are also interesting materials for catalytic applications and for fundamental studies of catalysis (Goldwasser, M. R., 2005).

Catalysis is a general property of matter, and there is seemingly always some mineral species that will catalyze a given reaction. However, most catalysis is specific, and for each given reaction or family of reactions there is only a small group of mineral species that are favorably endowed with appropriate catalytic properties. Empirical classifications of which mineral catalysts catalyze different types of reactions that appear in general articles and treatises on catalysis merely summarize this specificity. The reactions are grouped according to one criterion and the mineral species according to another and for each family of reactions there is one or more group of minerals that offers exceptional catalytic activity. Generally, reactions are grouped on the basis of either the use of a common reactant, a functional similarity of reactants, or because they follow similar reaction mechanisms. Mineral species are generally classified according to their chemical and physical properties or according to the position of their constituent atoms in the Periodic Table. Sabatier established the first empirical classifications in the broadest sense. After that, as researchers specialized, the correlations summarizing the results of experimental work became progressively narrower. Only one family of reactions or catalyst species was considered, but these narrower correlations became more precise due to a more quantitative definition of the catalysts and the exploitation of kinetics in the experimental results. A very general correlation is based on the correspondence between the three main classes of solid catalysts, namely metals (such as Fe, Ni, Co), semi-conducting oxides (metal oxides and sulfides, such as NiO, V_2O_5, MoS_2), and isolating oxides (such as zeolites, perovskites, acids). Perovskite structures form an important family of crystals, which are known as double oxides or mixed-metal oxides and include metal oxides, halogenated metal complexes, metal carbides, and metal nitrides.

In recent years, several groups reported the formation of acetic acid from carbon dioxide and ethane using a solid catalyst. Because ethane is a cheap, readily available raw material, the direct catalytic oxidation of ethane would be a very attractive route for the production of acetic acid. For this reason several oxide catalysts have been tested by various groups for the conversion of ethane to acetic acid (Thornsteinson et al., 1978; Merzouki et al., 1992; Kitson, 1993; Hallett, 1991; Tessier et al., 1995; Blum et al., 1994).

The large availability of ethane has stimulated investigations on its catalytic conversion into acetic acid. Thorsteinson et al. (1978) were the first authors to observe the formation of acetic acid by working at 325°C and 20.4 atm with a Mo-V catalyst. For a while, very little academic work was done on the formation of acetic acid from ethane when Merzouki et al. (1993) screened some V and Mo oxide catalysts and tried to improve the catalytic performance of Mo-V catalysts. Other vanadium-based catalysts were also studied by Tessier et al. (1995) and Roy et al. (1996) examined the influence of molybdenum. Numerous studies have been conducted on the oxidation of ethane to acetic acid to find other catalysts, as shown in several reviews (Ruth et al., 1998; Linke et al., 2002). Recently, a significant number of researchers have made great efforts to achieve the synthesis of acetic acid from ethane and carbon dioxide and oxygen (Smejkal et al., 2005; Linke et al., 2002). Finally, the ethane direct oxidation process was compared to acetic acid production by methanol carbonylation (currently used to obtain acetic acid) and the investment and production costs are discussed (Smejkal et al., 2005). The synthesis of acetic acid from natural gas and CO_2 in the presence of O_2 has been investigated by Huang et al. (2004).

In this work, we have studied the properties of some ABO_3 structures, such as $LaMoO_{3+\delta}$ and $LaVO_{3+\delta}$, and the influence of the presence of certain elements, such as Mo or V, on ternary perovskite-type structures containing La, Mo, and V. To study the influence of the chemical composition and the calcination conditions on the microstructure and catalytic behavior of $LaMo_xV_{1-x}O_{3+\delta}$ perovskites on the synthesis of acetic acid through the reforming of ethane, various characterization techniques have

been applied, namely: Fourier-transform infrared (FT-IR) spectroscopy, X-ray diffraction analysis (XRD), energy-dispersive X-ray spectrometry (EDS) coupled with scanning electron microscopy (SEM), thermogravimetric analysis (TGA–DTA), specific surface area determination (BET), and carbon analysis (CA). Post-test characterizations were also performed to obtain information about the active phase of the perovskite during the reactivity tests.

EXPERIMENTAL PROCEDURE

Preparation of the Perovskite Mixed Oxides

Perovskites may be prepared by different methods: ceramic or soft chemistry (impregnation, co-precipitation, or sol–gel processing). Other techniques, such as spray-drying, freeze-drying, or hydrothermal synthesis, are also possible (Campanati et al., 2003). For the present work, catalysts were prepared by a sol–gel method using distilled water as solvent. Catalysts were prepared in accordance with the formula $LaMo_xV_{1-x}O_{3+\delta}$, with x varying from 0 to 1 in increments of 0.1. Precursor solutions were prepared separately by dissolving the raw materials in hot distilled water. Seven kinds of $LaMo_xV_{1-x}O_{3+\delta}$ perovskite powder catalysts (x = 0, 0.1, 0.3, 0.5, 0.7, 0.9, and 1.0, with $0.5 < \delta < 1.5$) were prepared by an alkoxide technique. The reagents used were: lanthanum nitrate hexahydrate $La(NO_3)_3{\cdot}6H_2O$, vanadium(IV) oxide acetylacetonate $C_{10}H_{14}O_5V$, and ammonium heptamolybdate tetrahydrate $(NH_4)_6Mo_7O_{24}{\cdot}4H_2O$. All of the starting compounds were of purity > 99%. The initial source of the metallic element was separately introduced in hot distilled water until the formation of a limpid solution. Ammonium heptamolybdate is sparingly soluble in water. It was dissolved in the minimum volume of water. After dissolution, the two solutions were mixed and stirred for 120 minutes. Water was then distilled off until a resin was formed, which hardened on cooling. A scheme for the sol–gel preparation is illustrated in Figure 1. The resulting gel was dried at 90°C overnight and calcined at 750°C for 4 h (Parvary et al., 2001); catalysts were calcined by increasing the temperature at a rate of 3°C/min from 25°C in a static air atmosphere.

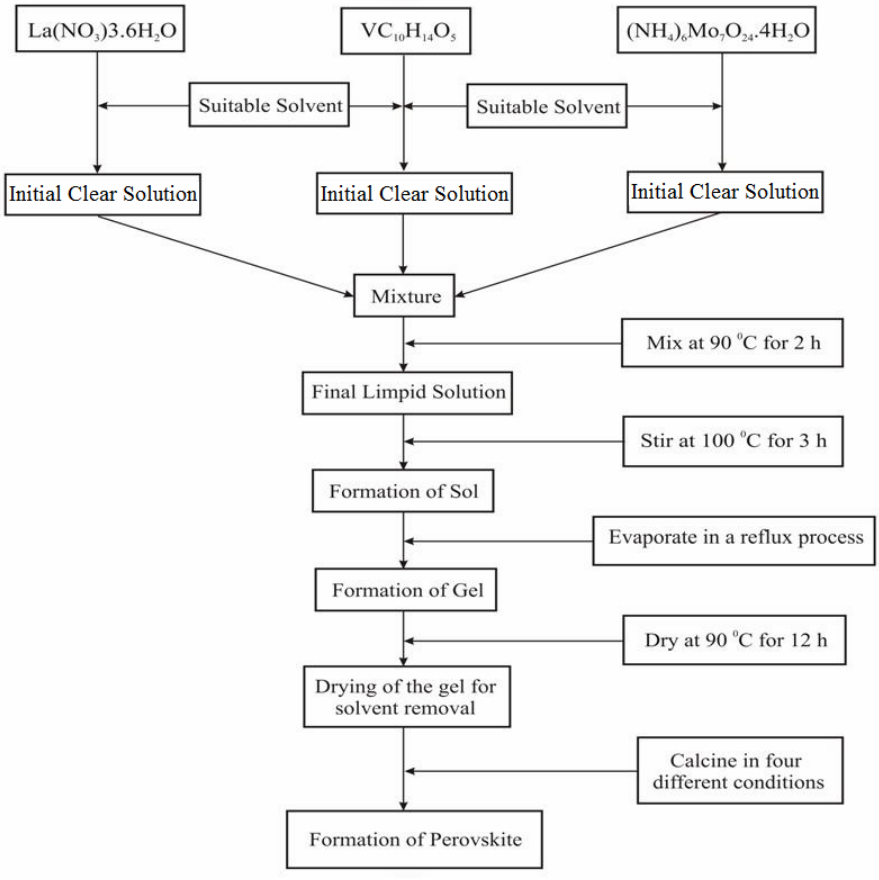

Figure 1: Preparation of the perovskite catalysts by a sol–gel process.

Fresh/Used Catalyst Characterization

The catalysts were characterized by the application of several techniques. We studied both the structure of the resins obtained following the gel formation process and the formation of precursors in the aqueous solution by means of Fourier-transform infrared spectroscopy (FT-IR) using a Shimadzu 8400S spectrophotometer. The perovskite (3 wt. %) was mixed with KBr and pressed to form a disc weighing about 100 mg and of thickness 1 cm. All samples were chemically analyzed by scanning electron microscopy (SEM) in conjunction with energy-dispersive spectroscopy (EDS). This determination of the chemical compositions of the samples allowed assessment of the structure and the homogeneity of the prepared materials. Morphological observations by SEM of catalysts calcined at 750°C were made with a Philips XL30 microscope and EDS analysis was carried out using a DS DX-4 analysis system. An accelerating voltage of 30 kV was used. A very thin Au deposit was applied to improve the conductivity of the sample. The crystalline phases in the samples were determined by X-ray diffraction (XRD) analysis. Data were collected at room temperature using a Philips PW-1800 diffractometer employing Cu-K_α radiation ($\lambda = 1.5406$ Å) and operating at 40 kV and 30 mA. All fresh and used catalysts were submitted to XRD analysis to ascertain whether the desired perovskite structure had actually been obtained by determining the crystalline phases and calculating the lattice parameters. For all samples, scattering intensities were measured over the angular range $4° < 2\theta < 90°$ with a step size (2θ) of 0.03° and a count time of 2 s per step. Thermal analysis of the gels to determine their weight losses was carried out on a TA 2960 simultaneous thermogravimetric analysis (TGA) and differential thermal analysis (DTA) apparatus in air atmosphere from room temperature to 750°C. For this, 10 mg samples of gels dried at 50°C for 24 h were used; the heating rate program used was 2°C/min to 400°C, and then 5°C/min from 400°C to 750°C. Specific surface area measurements were carried out by the BET method based on N_2 physisorption capacity at 77 K using a Micromeritics Flowsorb apparatus, the instrument operating in single-point and multi-point modes. Prior to analysis, the samples were degassed for 2 h at 150°C. For bulk and nonporous catalysts, such as those of the perovskite type, the specific surface area can be directly related to the average crystal size. The total amount of carbon deposited on the catalysts during ethane-reforming reactions was measured by carbon analysis (CA) using a Leco CS-444 thermal analyzer. Samples were heated from ambient temperature to burning in an oven and the amount of gas produced was determined by means of a quadruple mass spectrometer.

RESULTS AND DISCUSSION

Evaluation of the Stability of the Perovskites

The versatile properties of perovskites are of great interest, and this aspect is emphasized here for the ABO_3 and $AB_yB'_{1-y}O_3$ structures. For the reasons given above, we describe some characterizations of the reactivity of these systems in heterogeneous catalysis, to highlight the diversity of their behavior and hence the richness of their potential applications. Table 1 shows some important strategies for obtaining some stable structures of perovskite catalysts based on calculated results. The distortions of the perovskite (ABO_3) structure with respect to the ideally cubic stable one are controlled by the tolerance factor (Equation 1), where r_A, r_B are the ionic radii for 12 and 6-coordination, respectively, and r_O is the oxygen anion radius in six fold coordination (Voorhoeve, et al., 1977; Ran, et al., 2005).

Table 1: Stability of perovskites according to the tolerance factor (*t*).

X	La			Mo			V			Tolerance Factor
	CN[a]	R[b]	X	CN[a]	R[b]	X	CN[a]	R[b]	X	
0	12	1.36	3	-	-	-	8	0.72	4	0.920
0.1	12	1.36	3	6	0.59	6	8	0.72	4	0.926
0.3	12	1.36	3	6	0.59	6	8	0.72	4	0.937
0.5	12	1.36	3	6	0.59	6	8	0.72	4	0.949
0.7	12	1.36	3	6	0.59	6	8	0.72	4	0.961
0.9	12	1.36	3	6	0.59	6	8	0.72	4	0.974
1	12	1.36	3	6	0.59	6	-	-	-	0.980

[a] Coordination number
[b] Ionic radius

The rare earth cations are replaced in the A-site and transition metal cations are substituted in the B-sites. The catalytic activity of the perovskite structure can be improved by substituting some of the B-sites with B'-sites (Tejuca et al., 1993; Tanaka et al., 2003; Nakamura et al., 1983; Nitadori et al. 1985). It is necessary to calculate tolerance factors for each structure to investigate the stability in each case. This table shows possible stability of perovskite type which is loaded with lanthanum, molybdenum, and vanadium. Due to the improving effects of Molybdenum, and Vanadium on the ethane reforming reaction, their impacts were investigated.

The tolerance factor can be qualitatively used as a measure of bond length mismatch in the cubic perovskite structure. On the other hand, for ionic crystals, internal lattice energy is considered to be the net result of both a long-range electrostatic force and a short-range force, of which the repulsion force represents the main component, in addition to van der Waals, vibration, and covalent contributions (Takayawa-Muromachi et al., 1993).

Physico-Chemical Characteristics of Perovskites

The present perovskite systems have been mainly characterized by XRD and FT-IR analyses. The FT-IR spectra of the gels obtained from solutions of the starting salts in water show no change in the band positions of the gel components $VC_{10}H_{14}O_5$, $(NH_4)_6Mo_7O_{24}$, and $La(NO_3)_3$, indicating no deposition or reaction between the solvent and the starting salts. Figure 2 shows the peak positions of the starting salts and Figure 3 shows the corresponding FTIR spectra of the gels. Similarity of bands positions in FT-IR spectra for starting salts and the produced gel shows the presence of unchanged primary molecules in the gel.

It can be concluded that, after dissolution in water and hydrolysis, the salts exist in the gel and so the gel is simply a mixture of the starting salts. In the gel IR spectra of $LaMo_xV_{1-x}O_{3+\delta}$, the main FT-IR bands were observed at 1630, 1040, and 817 cm^{-1} for La; at 1402, 890, and 564 cm^{-1} for Mo; and at 1357, and 949 cm^{-1} for V. These band positions are in good agreement with the IR spectral bands (cm^{-1}) of the starting materials. XRD and FT-IR spectra of the $LaMo_xV_{1-x}O_{3+\delta}$ precursor were recorded to confirm the presence of the expected perovskite-like oxide. These analyses prove that the sol–gel method produces solids with high crystallinity, homogeneity and purity. According to Figure 3, the FT-IR spectra of this material showed two bands characteristic of the perovskite-like structure: ν_1 localized between 900 and 800 cm^{-1} and ν_2 at 600 cm^{-1}. The first band ν_1 is attributed to the stretching vibration and the second one ν_2 to the deformation produced by changes in the bond angles between oxygen atoms of the perovskite-like structure

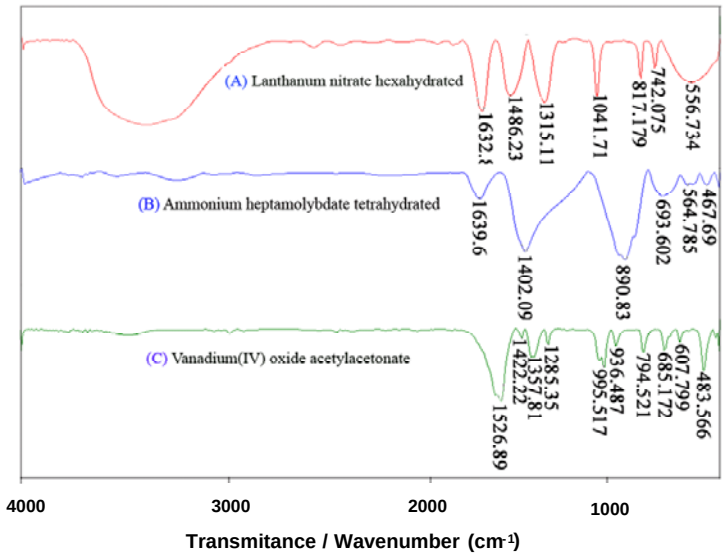

Figure 2: IR spectra and bands (cm^{-1}) of the starting salts.

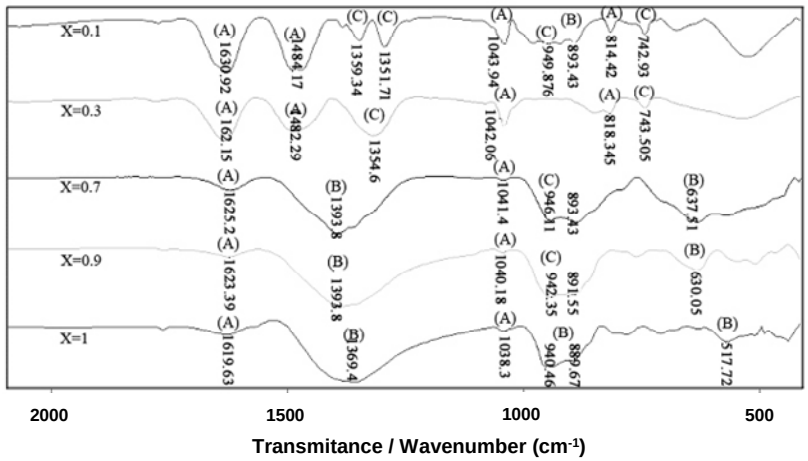

Figure 3: IR spectra and bands (cm^{-1}) of the $LaMo_xV_{1-x}O_{3+\delta}$ gel. A, B, and C refer to the starting materials shown in Figure 2.

The TGA and DTA curves of this sample are shown in Figure 4. The DTA curve features three major peaks, two of which are endothermic while the third is exothermic. The first endothermic peak appears at a low temperature of about 100°C, This weight loss is attributed to the deadsorption of humidity on the exterior surface of the powders; residual water can be desorbed from the surface during heating the sample by the TG analyzer. The second stage occurs at about 250°C and is due to the removal of hydroxyl groups bonded to the surface of the lanthanum, corresponding to a weight loss attributed to humidity in the interior pores of the powder desorbed from the pores during the TGA processing. The exothermic peak at about 400°C may be attributed to the crystallization of amorphous lanthanum. Simultaneously, the TGA curve levels off at about 450°C, indicating that the organic residues have been completely removed, as confirmed by the FT-IR results.

The BET surface areas of the catalysts were found to be between 2.64 m^2/g ($x = 0.1$) and 5.13 m^2/g ($x = 1.0$) following calcinations at 750°C (Table 2). Figure 5 shows the adsorption isotherms for the samples. It can be seen that the volume of adsorbed gas increases with increasing molybdenum content in the samples. Thus, the total pore volumes of the molybdenum-rich samples are higher than those of the others (see Figure 5 and Table 2). BET specific surface areas measured after calcination for the different elemental compositions of these five samples, which relate to the crystallization, are in good accordance with the results of X-ray analyses.

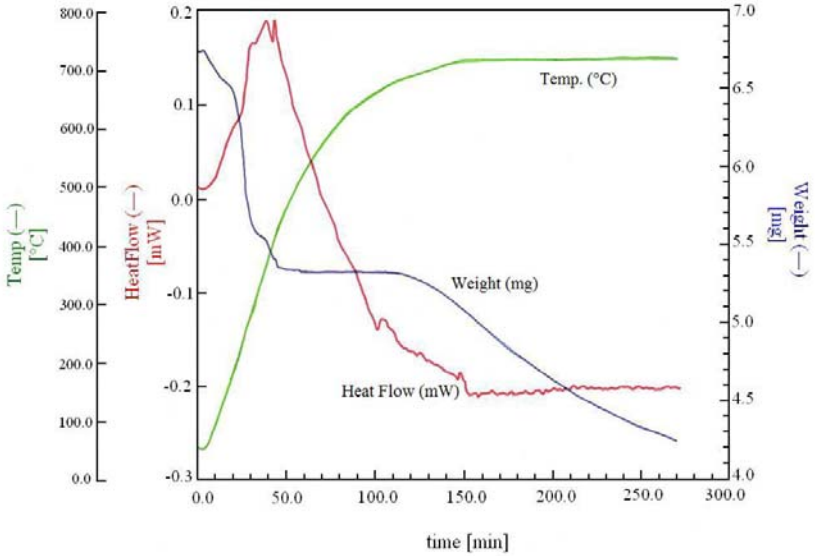

Figure 4: Profile TGA/DTA analysis for $LaMo_{0.7}V_{0.3}O_{4.2}$ calcined at 750°C.

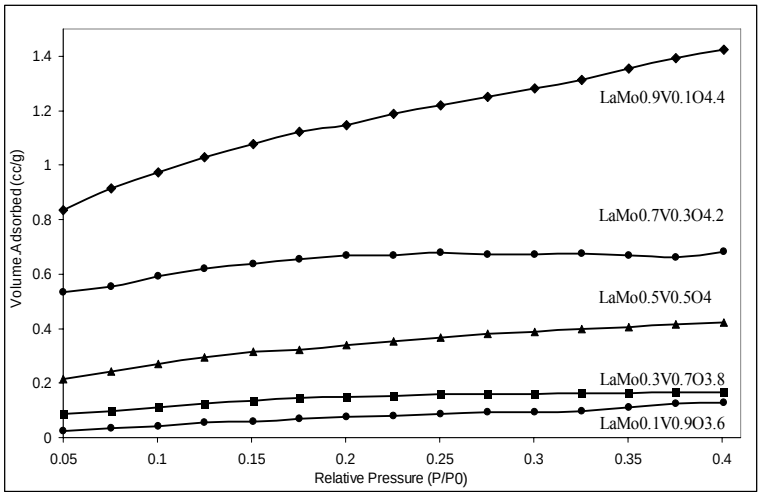

Figure 5: Adsorption isotherms of the $LaMo_xV_{1-x}O_{3+\delta}$ calcined at 750°C.

Table 2: Structural properties of the catalysts.

Composition of perovskite (X)	Multi point (BET) m^2/g	Single Point (BET) m^2/g	Pore Volume (cm^3/g)	Volume adsorbed (cc/g)	Lattice parameters Exp.(Å)[a]	Lattice parameters Act.(Å)[b]
1.0	5.1	5.0	0.0153	1.731	6.839	6.853
0.9	4.0	3.9	0.0098	1.424	6.724	6.731
0.7	3.2	3.1	0.0075	0.683	6.610	6.623
0.3	2.8	2.8	0.0032	0.421	6.513	6.589
0.1	2.6	2.5	0.0019	0.166	6.429	6.450

[a]Experimental
[b]Actual values measured from the refinement XRD pattern.

XRD patterns of the $LaMo_xV_{1-x}O_{3+\delta}$ mixed-oxide series ($x = 0.1$, 0.3, 0.5, 0.7, and 0.9) calcined at 750°C are shown in Figure 6a. As indicated in this figure, crystal phases related to Mo^{6+} ($La_2Mo_2O_9$) and V^{5+} ($LaVO_4$) are present. However, the 2θ values of these peaks differ somewhat compared to the standard peaks. For this reason, we conclude that the samples are mixtures of these two different crystals. The series was compared to $LaVO_4$ and $La_2Mo_2O_9$ reference diagrams. In each case, a perovskite phase was seen to be obtained (Figure 6a). However, for ternary La-Mo-V systems, a progressive and regular shift of the structure peaks between those of $LaVO_4$ and $La_2Mo_2O_9$ with increasing x was noted. This indicates the formation of a solid solution of $La_2Mo_2O_9$ and $LaVO_4$ in all proportions ($0 \leq x \leq 1$). An enlargement of the 2θ diagram between 27° and 28° shows this progressive shift for the most intense diffraction peak of some $LaMo_xV_{1-x}O_{3+\delta}$ structures (Figure 6b).

As indicated in Figure 6a, for vanadium-rich samples ($x = 0.1$, 0.3, and 0.5), some weak diffraction lines related to La, Mo, and V oxides are present. It is also evident that in molybdenum-rich samples the conditions for the formation of ternary perovskite are more favored than in the other samples. A perovskite phase is therefore formed in these samples. We consider that the formation of the ternary structure is directly related to competition between the formation of bimetallic and ternary perovskites ($LaVO_4$ and $La_2Mo_2O_9$ for calcinations at 750°C). This result confirms the formation of a solid La-Mo-V solution, and that the variation in the lattice parameter may be used to define the molybdenum content for each obtained perovskite and, in particular, to evaluate the molybdenum content after the reactivity tests.

The lattice parameter, a, was calculated from the seven most intense diffraction lines, assuming a pseudo-cubic structure. It increases linearly with x between 6.429 and 6.839 Å, corroborating the solid solution formation. The obtained curve enables determination of the molybdenum content (x) of the perovskite and may thus be used as a calibration system to evaluate the possible migration of molybdenum out of the structure during the catalytic tests (Table 2).

For an ideal cubic perovskite structure, $t = 1$ and there is apparent contraction of the octahedral sub-lattice with respect to the ideal structure. Assuming

that all the ions are hard spheres, the lattice parameter (a) of the cubic perovskite is given by:

$$a = \frac{\lambda(\sqrt{h^2 + k^2 + l^2})}{2\sin\theta} \quad (2)$$

In Equation (2), the lattice parameter is determined by the length of the bond B-O, since the B-O-B ion arrangement is more compact than the A-O-A arrangement in the ideal ABO_3 structure, as found in $LaNiO_3$ and $LaAlO_3$ (Parvary et al., 2001). In the present catalysts, the B-site is occupied by two different ions, Mo and V. When Equation (2) is used, the obtained lattice parameters are higher compared to the actual values of a measured from the refined XRD pattern. This deviation could be due to several factors, such as deviation from the ideal cubic perovskite structure. An average multiplication factor has been introduced into Equation (2) in order to obtain a value closer to the measured one. This factor is estimated from the ratio between the measured values and the values obtained from Equation (2), and the expression becomes:

$$a = \left(\frac{\lambda(\sqrt{h^2 + k^2 + l^2})}{2\sin\theta}\right)0.996 \quad (3)$$

Equation (3) was then used to calculate the theoretical lattice parameter for the structures with various molybdenum contents (Table 2), assuming an ideal cubic perovskite structure.

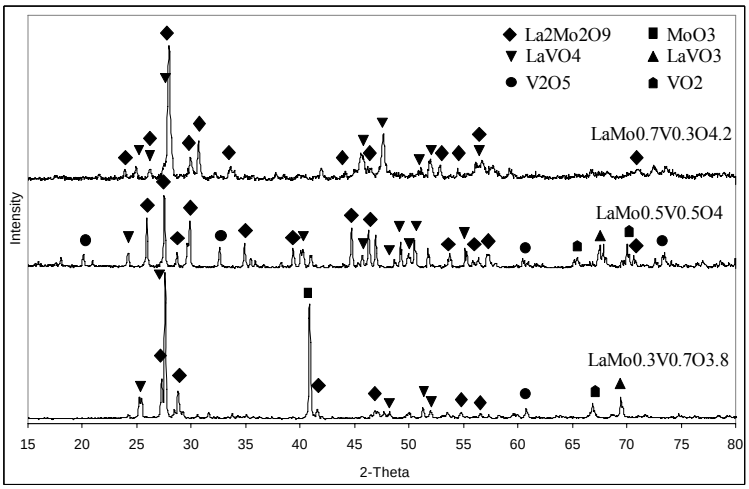

(a)

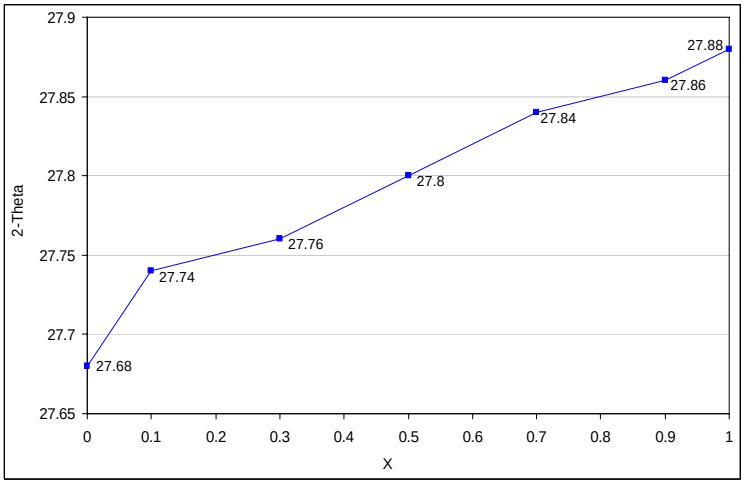

(b)

Figure 6: (a) XRD patterns of $LaMo_xV_{1-x}O_{3+\delta}$ mixed-oxide perovskite. (b) Evolution of the position of the highest XRD peak.

Scanning electron micrographs of $LaMo_{0.7}V_{0.3}O_{4.2}$ before and after the reactivity tests are shown in Figure 7. The SEM of the fresh catalyst (Figure 7a) shows porosity of this structure (grains of diameters ranging from 0.5 to 1 μm). The surface of the catalyst presents a spongy discrete particle appearance. The formation of a carbon deposit on the catalysts under the reaction conditions was evidenced by SEM observations. Micrographs of a catalyst sample before and after tests on the reforming of ethane after 15 h reaction at 850°C in the fix bed reactor are shown in Figures 7a and 7b, respectively. After reactivity test, the porosity observed on used catalyst disappears, more compact grains are formed and the local crystallinity is increased and carbon can be observed on the surface. The comparison of Figures 7a and 7b clearly show differences in the amount of coke deposited on the two samples (fresh and used catalyst). Carbon can clearly be seen on the surfaces of the grains. SEM observations after the tests revealed the nature of the carbon species, that is, carbonaceous layers on the surface of the grains (Figure 7b), as also evidenced by EDS, were very low (lower than 0.3 wt %). The combined XRD and SEM characterizations demonstrate the formation of a homogeneous La-Mo-V solid solution.

Energy-dispersive X-ray spectroscopy (EDS) coupled with SEM measurement was carried out at different points along the samples using a broad focus beam (200 nm) (1) to determine the mean element proportions of the sample, and a small focus beam (14 nm) (2–5) to ascertain the homogeneity of the preparation of $LaMo_{0.7}V_{0.3}O_{4.2.}$ The chemical compositions of the catalysts determined from the EDS data were very similar to those calculated by applying the only criterion that needs to be fulfilled in order to form a perovskite-type structure, that is, the ionic radii requirement introduced by Goldschmidt (Goldwasser, M. R., 2005), the so-called tolerance factor (t) defined by Equation (1). The elemental compositions in the series of $LaMo_xV_{1-x}O_{3+\delta}$ mixed oxides determined by EDS were invariably in good agreement with the theoretical values.

Table 3 shows the calculated and theoretical chemical compositions of the seven synthesized mixed-oxide perovskites. The average theoretical composition (EDS) has also been calculated from the proportion of molybdenum and vanadium cations in the B-sites of the perovskite, which was varied between $x = 1$ for $LaMoO_{3+\delta}$ and $x = 0$ for $LaVO_{3+\delta}$. There is very good agreement between the experimental and theoretical (EDS) perovskite compositions for $LaMo_xV_{1-x}O_{3+\delta}$, whereas the slight difference in elemental composition is probably due to a difference in stoichiometry with regard to oxygen. The value of x strongly depends on the preparation conditions and has not been precisely measured.

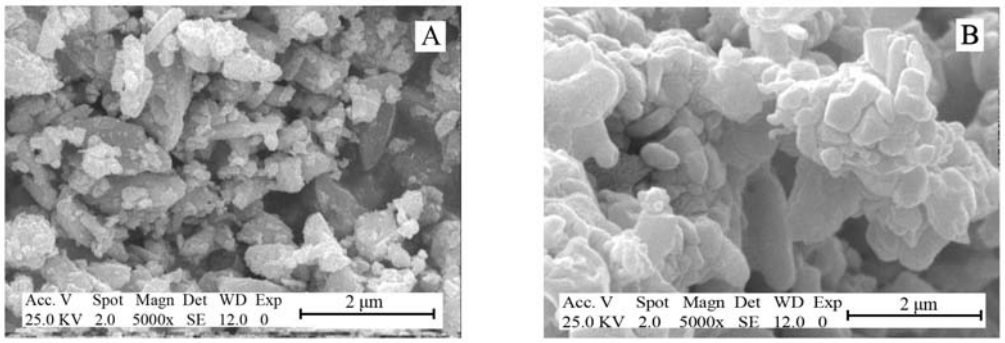

Figure 7: Scanning electron micrograph for $LaMo_{0.7}V_{0.3}O_{4.2}$ A) before at 750°C, B) after calcinations at 750°C.

Table 3: Comparison of the theoretical and experimental (EDS) perovskite compositions.

X	Theoretical Composition	La%		Mo%		V%	
		Cal.[a]	Exp.[b]	Cal.[a]	Exp.[b]	Cal.[a]	Exp.[b]
1	$LaMoO_{4.5}$	59.14	58.31	40.85	41.68	0	0
0.9	$LaMo_{0.9}V_{0.1}O_{4.4}$	60.30	61.19	37.46	36.01	12.24	12.80
0.7	$LaMo_{0.7}V_{0.3}O_{4.2}$	62.74	62.41	30.31	31.20	6.95	6.39
0.5	$LaMo_{0.5}V_{0.5}O_4$	65.41	63.93	22.58	20.71	12.01	15.35
0.3	$LaMo_{0.3}V_{0.7}O_{3.8}$	68.31	67.18	14.15	13.02	17.54	19.80
0.1	$LaMo_{0.1}V_{0.9}O_{3.6}$	71.47	72.39	4.93	3.91	23.60	23.70
0	$LaVO_{3.5}$	73.16	72.54	0	0	26.84	27.46

[a]Calculated
[b]Experimental

Careful examination of the main diffraction peak of $LaMo_{0.7}V_{0.3}O_{4.2}$ after 15 h of reaction shows that the peak position is almost unchanged, thus indicating very good stability. The results of SEM and EDS analyses of the used catalysts were in agreement with the carbon analysis results, showing a higher degree of coke deposition with increasing pressure and decreasing temperature. EDS analysis confirmed that the homogeneity of the catalyst after the test was similar to that before the test for $x = 0.7$. At $x = 0.7$, localized regions of higher molybdenum concentrations are formed. We also measured the amount of carbon after the same test duration of 15 h. The minimum carbon formation on the samples was found to be 0.3 wt% of the total catalyst mass for $LaMo_{0.7}V_{0.3}O_{4.2}$ used for the ethane-reforming reaction with $C_2H_6/CO_2 = 1$ at atmospheric pressure.

CATALYTIC PERFORMANCE

Catalytic tests on the direct synthesis of acetic acid were performed at 8 bar. The reaction conditions applied were as follows: fixed-bed stainless steel reactor (6.6 mm I.D.); inlet temperature: 450–850°C; flow rates of components: C_2H_6:CO_2:O_2 = 2:1:2, the flow rates of the components were: C_2H_6: 5 cc/min; CO_2 2.5 cc/min; O_2 5 cc/min; N_2 40 cc/min; weight of catalyst: 200 mg.

Catalysts with various molybdenum oxide contents were tested for their activities in the reforming of ethane. Reactions were performed with the perovskite in a fixed-bed reactor following a temperature program. The results of the reaction performed at 8 bar on a sample of $LaMo_{0.7}V_{0.3}O_{4.2}$ calcined at 750°C are presented in Table 4 (ramps 1, 2, and 3 are increasing). A change in the catalytic behavior is observed between the first heating and cooling ramps. $LaMo_{0.7}V_{0.3}O_{4.2}$ shows an initial level of C_2H_6 conversion of no less than 55.3%, while in the second step at 850°C (during the second cycle) it displays a higher value (C_2H_6 conversion of 68.4%). During the aging step, a further increase is observed up to 78.3% ethane conversion. Table 4 shows the relationship between CH_3COOH selectivity and reaction temperature.

As can be seen in this table, CH_3COOH production starts at 550°C during the first ramp and it increases up to approximately 8.24%. $LaMo_{0.7}V_{0.3}O_{4.2}$ shows an initial degree of CH_3COOH selectivity of 3.49%, but in the second step it shows a higher value of 8%. Reduction of the surface activates the catalyst and hence acetic acid production continues during the cooling ramp. The trend in the third heating ramp is similar to that in the second ramp; the CH_3COOH selectivity during the aging step reaches a maximum value of about 8.24% at 850°C. The same phenomenon as before is observed for the CH_3COOH yield. Table 3 shows that the CH_3COOH yields are in excess of 6.45% for $LaMo_{0.7}V_{0.3}O_{4.2}$ at 850ºC.

For the other samples ($0.1 < x < 0.5$), high activities are obtained at 850°C in the three cycles, but the CH_3COOH selectivity and yields are lower than 3% and 2%, respectively. This shows that the samples with higher x values ($x > 0.5$) are more active and selective than those with lower x values ($x < 0.5$). As mentioned previously, the structure of the molybdenum-rich samples ($x > 0.7$) is of a perovskite type, but in the other samples metal oxide and perovskite structures co-exist. For this reason, carbon formation during reactions catalyzed by the molybdenum-rich samples is lower than that with the other samples. The catalyst $LaMo_{0.7}V_{0.3}O_{4.2}$ shows good activity and stability after 15 h of direct synthesis of acetic acid from ethane at 750°C.

Table 4: Effect of temperature program on catalytic performance of the $LaMo_{0.7}V_{0.3}O_{4.2}$ catalyst.

Ramp	**1**				**2**				**3**			
Temperature °C	**550**	**650**	**750**	**850**	**550**	**650**	**750**	**850**	**550**	**650**	**750**	**850**
Con. (C_2H_6) %	4.36	14.9	42.2	55.3	10.9	35.9	48.1	68.4	20.4	54.1	70.5	78.3
Sel. (CH_3COOH) %	1.94	2.14	2.03	3.49	5.73	5.11	5.82	8.07	7.0	6.84	7.13	8.24
Yield (CH_3COOH) %	Trace	0.32	0.85	1.93	0.62	1.83	2.80	5.52	1.43	3.70	5.03	6.45

CONCLUSIONS

This work has highlighted the potential of perovskite systems of the type $AB_yB'_{y-1}O_3$ as heterogeneous catalysts for ethane-reforming reactions. The synthesis of $LaMo_xV_{1-x}O_{3+\delta}$ perovskites has been investigated in an attempt to overcome the disadvantages of the solid-state route. Due to its advantages of high purity products, good chemical homogeneity, and lower calcinations temperatures as compared with the solid-state chemistry route, the sol–gel process provides an attractive and effective alternative for synthesizing materials with better control of morphology. A gel with a high degree of homogeneity can be obtained from a solution of the appropriate precursors. Perovskites not only fulfill the stability requirements, but by further reduction of the B-site cations, which remain distributed throughout the structure, they can be used to obtain well-dispersed and stable metal particle catalysts. We have demonstrated that $LaMo_xV_{1-x}O_{3+\delta}$ mixed oxides ($0 < x < 1$) obtained by means of a sol-gel related method efficiently catalyze the ethane dry reforming reaction. Compounds of the series $LaMo_xV_{1-x}O_{3+\delta}$ have been successfully prepared using water as the solvent and lanthanum nitrate, vanadium(IV) oxide acetylacetonate, and ammonium heptamolybdate as raw materials. Characterizations by SEM and XRD have demonstrated the formation of La-Mo-V solid solutions, and good homogeneity of the prepared systems has been proved by the constancy of local elemental distributions determined by EDS. These interesting properties are favourable for the application of these mixed perovskite $LaMo_xV_{1-x}O_{3+\delta}$ systems as catalysts. It has been demonstrated that these systems may be used in ethane dry reforming, and that they are more selective than other catalysts in producing acetic acid.

Such characterization of heterogeneous catalysts of the type $LaMo_xV_{1-x}O_{3+\delta}$ has shown that subjecting appropriate precursors to calcinations under optimal conditions (time and temperature) can yield mixed oxides with the desired perovskite structure and with notable properties for their application as heterogeneous catalysts.

Although the development of perovskite catalysts has previously been treated in detail (Parvary et al., 2001), at the end of this overview, it may be useful to briefly summarize the main studies of perovskite systems and their application in catalysis. It should be noted that, currently, the preparation of perovskite catalysts, especially with regard to the specific perovskite structure, is almost totally approached on a scientific basis, exploiting knowledge derived from other related sciences. Heterogeneous catalysis is indeed a field where new challenges appear continuously, more and more charming and intriguing. Together with the continuous improvement in the area of the preparation of catalysts tailored for specific reactions and/or processes, mention should also be made of the impressive increase in the application of computational methods for the preparation, characterization, and testing of perovskite catalysts, which should facilitate the discovery of new catalyst compositions and applications.

ACKNOWLEDGEMENTS

The authors are highly indebted to the staff of the Iranian Energy and Material Research Center for their cooperation in characterizing the samples.

REFERENCES

Bernier, Mm. J. C., Sévèque, F., Delamoye, P., and Poix, P., Proprietes ferrimagnetiques des perovskites de type $Sr_3U_{1-x}W\ Fe_2O_9$. Solid State Communications, 9, 1225 (1971).

Blum, P. R., and Pepera, M. A., (The Standard Oil Corp.), U.S. Patent 5,300,682 (1994).

Campanati, M., Fornasari, G., and Vaccari, A., Fundamentals in the preparation of heterogeneous catalysts. Catalysis Today, 77, 299 (2003).

Goldwasser, M. R., Rivas, M. E., Pietri, E., Pérez-Zurita, M. J., Cubeiro, M. L., Grivobal-Constant, A., and Leclercq, G., Perovskites as catalysts precursors: synthesis and characterization. Journal of Molecular Catalysis A: Chemical, 228, 325 (2005).

Goldwasser, M. R., Rivas, M. E., Lugo, M. L., Pietri, E., Pérez-Zurita, J., Cubeiro, M. L., Griboval-Constant, A., and Leclercq, G., Combined methane reforming in presence of CO_2 and O_2 over $LaFe_{1-x}Co_xO_3$ mixed-oxide perovskites as catalysts precursors. Catalysis Today, 107, 106 (2005).

Goldwasser, M. R., Rivas, M. E., Pietri, E., Pérez-Zurita, M. J., Cubeiro, M. L., Gingembre, L., Leclercq, L., and Leclercq, G., Perovskites as catalysts precursors: CO_2 reforming of CH_4 on $Ln_{1-x}Ca_xRu_{0.8}Ni_{0.2}O_3$ (Ln=La,Sm,Nd). Applied Catalysis A: General 255, 45 (2003).

Goldschmidt, V. M., Skr. Nor. Videnk. Akad, Kl. 1, Mat. Naturvidensk Kl. 8 (1926).

Hallett, C. (BP Chemicals), Europ. Patent 0 480 594 A2 (1991).

Hazen, R. M., American journal of science, 288A: 242 (1988).

Huang, W., Zhang, C., Yin, L., and Xie K., Direct Synthesis of Acetic Acid from CH_4 and CO_2 in the Presence of O_2 over a V_2O_5-$PdCl_2/Al_2O_3$ Catalyst. Journal of Natural Gas Chemistry. 13, 113 (2004).

Kattack, C. P., and Wang, F. F. Y., Handbook of the Physics and Chemistry of the Rare Earths. Ed. Gschneider, K. A. and Enging, L., North Holland Publ., Amsterdam, p. 525 (1979),

Kitson, M. (BP Chemicals Ltd.), U.S. Patent 5,260,250 (1993).

Linke, D., Wolf, D., Baerns, M., Timpe, O., Schlogl, R., Zey, S., and Dingerdissenz, U., Catalytic Partial Oxidation of Ethane to Acetic Acid over $Mo_1V_{0.25}Nb_{0.12}Pd_{0.0005}O_x$. Journal of Catalysis 205, 16 (2002).

Merzouki, M., Taouk, B., Monceaux, L., Bordes, E., and Courtine, P., Catalytic Properties Of Promoted Vanadium Oxide In The Oxidation Of Ethane In Acetic Acid. Studies in Surface Science and Catalysis, 72, 165 (1992).

Merzouki, M., Taouk, B., Tessier, L., Bordes, E., and Courtine, P., Correlation Between Catalytic and Structural Properties of Modified Molybdenum and Vanadium Oxides in the Oxidation of Ethane in Acetic Acid or Ethylene. Studies in Surface Science and Catalysis, 75, 753 (1993).

Nakamura, T., Misono, M., and Yoneda, Y., Reduction-oxidation and catalytic properties of $La_{1-x}Sr_xCoO_3$. Journal of Catalysis, 83, 151 (1983).

Nitadori, T., Kurihara, S. and Misono, M., Catalytic properties of $La_{1-x}A'_xMnO_3$ (A′ = Sr, Ce, Hf). Journal of Catalysis**,** 98, 221 (1986).

Parvary, M., Jazayeri, S. H., Taeb, A., Petit, C., and Kiennemann, A., Promotion of active nickel catalysts in methane dry reforming reaction by aluminum addition. Catalysis Communication, 2, 357 (2001).

Pietri, E., Barrios, A., Gonzalez, O., Goldwasser, M. R., Pérez-Zurita, M. J., Cubeiro M. L., Goldwasser, J., Leclercq, L., Leclercq, G., and Gingembre, L., Perovskites as catalysts precursors for methane reforming: Ru based catalysts. Studies in Surface Science and Catalysis, 136, 381 (2001).

Ran, R, Wu, X., Quan, C., and Weng, D., Effect of strontium and cerium doping on the structural and catalytic properties of $PrMnO_3$ oxides. Solid State Ionics 176, 965 (2005).

Roy, M., Gubelmann-Bonneau, M., Ponceblanc, H., and Volta, J. C., Vanadium- molybdenum phosphates supported by TiO_2 anatase as new catalysts for selective oxidation of ethane to acetic acid. Catalysis Letter, 42, 93 (1996).

Ruth, K., Kieffer, R., and Burch, R., Mo–V–Nb Oxide Catalysts for the Partial Oxidation of Ethane. Journal of Catalysis 175, 16 (1998).

Smejkal, Q., Linke, D. and Baerns, M., Energetic and economic evaluation of the production of acetic acid via ethane oxidation. Chemical Engineering and Processing, 44, 421 (2005).

Takayama-Muromachi, E. and Navrotsky, A., Thermochemical Study of Ln_2O_3, T′-Ln_2CuO_4, and $Ln_2Cu_2O_5$ (Ln = Rare Earth). Journal of Solid State Chemistry, 106, 349 (1993).

Tanaka, H., and Misono, M., Advances in designing perovskite catalysts. Current Opinion in Solid State and Materials Science, 5, 381 (2001).

Tanaka, H., Mizuno, N. and Misono, M., Catalytic activity and structural stability of $La_{0.9}Ce_{0.1}Co_{1-x}Fe_xO_3$ perovskite catalysts for automotive emissions control. Applied Catalysis A: General, 244, 371 (2003).

Tejuca, L. G. and Fierro, J. L. G., Properties and Applications of Perovskite-Type Oxides, Edited by Marcel Dekker, New York, 289-306 (1993).

Tessier, L., Bordes, E., and Gubelmann-Bonneau, M., Active specie on vanadium-containing catalysts for the selective oxidation of ethane to acetic acid. Catalysis Today 24, 335 (1995).

Thorsteinson, E. M., Wilson, T. P., Young, F. G., and Kasai, P. H., The oxidative dehydrogenation of ethane over catalysts containing mixed oxides of molybdenum and vanadium. Journal of Catalysis, 52, 116 (1978).

Voorhoeve, R. J. H., Perovskite Oxides. Materials Science in Catalysis, Science, 195, 827 (1977).

Utaka, T., Al-Drees, S., Ueda, J., Iwasa, Y., Takeguchi, T., Kikuchi, R., and Eguchi, K., Partial oxidation of methane over Ni catalysts based on hexaaliminate- or perovskite-type oxides. Applied Catalysis A: General, 247, 25 (2003).